

Statistical Evaluation of Orientation Correction Algorithms in a Real-Time Hand Tracking Application for Computer Interaction

Neeranut Ratchatanantakit, Nonnarit O-larnnithipong^(\boxtimes), Pontakorn Sonchan^(\boxtimes), Malek Adjouadi^(\boxtimes), and Armando Barreto^(\boxtimes)

Department of Electrical and Computer Engineering, Florida International University, Miami, FL, USA

{nratc001, nolarnni, psonc001, adjouadi, barretoa}@fiu.edu

Abstract. A new approach to correct the orientation estimate for a miniature Magnetic-Angular Rate-Gravity (MARG) module is statistically evaluated in a hand motion tracking system. Thirty human subjects performed an experiment to validate the performance of the proposed orientation correction algorithm in both non-magnetically distorted (MN) and magnetically distorted (MD) areas. The Kruskal-Wallis tests show that the orientation correction algorithm using Gravity and Magnetic Vectors with Double SLERP (GMV-D), the correction using Gravity and Magnetic Vectors with Single SLERP (GMV-S) and the on-board Kalman-Filter (KF) performed similarly in non-magnetically distorted areas. However, the statistical tests show that, when operating in the magnetically distorted region, the level of error in the orientation estimates produced by the three methods is significantly different, with the proposed GMV-D method yielding lower levels of error in the three Euler Angles Phi, Theta and Psi. This indicates that the GMV-D method was better able to provide orientation estimates that are more robust against local disturbances of the magnetic field that might exist in the operating space of the MARG module.

Keywords: MARG · Inertial measurement unit · Gyroscope drift · Drift correction algorithm · Quaternion correction · Magnetic distortion · Hand motion tracking

1 Introduction

Over the past decade, the popularity of Virtual Reality (VR) and Augmented Reality (AR) has dramatically increased in many applications [1–5]. Computers are part of many aspects of human activity and users seek to interact with computers in ways that are natural and intuitive [6–8]. The available input devices like mice, game pads, joysticks and wands are commonly used to interact with computers but may require the user to perform highly artificial sequences of actions. Therefore, the ability for computer systems to have the real-time capability to capture user hand movement or hand motion tracking is an interesting option for users to interact more naturally with 3D interfaces and may

be a crucial step towards the improvement of the next generation of human-computer interaction systems.

An emerging approach for capturing the orientation of the hand is the use of Micro-Electro-Mechanical Systems (MEMS) Magnetic-Angular Rate-Gravity modules (MARGs). These miniature modules can be attached to multiple segments of an instrumented glove to monitor the different moving segments of the user's hand. In this initial development we have studied the use of a single MARG module (YEI 3-space Sensor) attached to the dorsal surface of a glove [9]. Simultaneously, a 3-camera IR-video tracking system (OptiTrack V120 Trio) is used in conjunction with the MARG module to provide position coordinates of the sensor. The 3D gyroscope in the MARG module measures its angular velocity and makes it possible to calculate the module's 3D orientation by quaternion (q) accumulation.

While this angle accumulation is the fundamental concept for orientation estimation using Inertial Measurement Units (IMUs), different types of gyroscopes are used in many industries and have a wide range of accuracy levels that tend to be in proportion to their price [10], from navigation systems in aviation to the MEMS gyroscopes used in portable devices (e.g., mobile phones). The different grades of gyroscopes have significantly different error and noise characteristics. MEMS gyroscopes may have significant offset levels in their outputs, which, furthermore, may not be exactly constant, but instead they may be slowly varying. This "bias offset error" can result in high levels of orientation tracking error, as the angular velocity readings have to be integrated over time to obtain orientation estimates. The resulting type of orientation error, called "drift," is a common effect that continues to grow through time as the sensor operates and keeps integrating the rotational speed measurements. Left uncorrected, the orientation drift is likely to result in orientation estimate errors that could soon render those estimates useless. In traditional inertial navigation systems, the inertial estimates of orientation and position are usually corrected periodically using information from external sources (e.g., GPS for outdoor position estimation). For our indoor, human-computer interaction application we sought to correct the gyroscope-based orientation estimates, expressed as a quaternion \hat{q}_G using the 2 other sensor modalities available in MARG modules: 3-axis accelerometer and 3-axis magnetometer.

For both, the accelerometer and the magnetometer, instantaneous readings in each of the 3 axes will evolve as the module changes orientation. We can rely on the assumption that the gravity vector will always be perpendicular to the floor of the environment where the MARG module is used. Therefore, the 3 currently measured accelerometer components should match the transformation of the gravity vector sensed initially (when the sensor is considered aligned with the inertial frame of reference), by application of the total orientation change estimated by the gyroscope operation, \hat{q}_G , from the initial orientation. If a difference exists, it may be hypothesized that it is due to error that has developed in \hat{q}_G (e.g., due to drift), and the 3 current accelerometer readings will offer a means to apply an accelerometer-based correction to \hat{q}_G . However, this reasoning is correct, and the accelerometer-based correction is adequate if, at the current time, the accelerometers are only recording the acceleration of gravity. This requires that the MARG module be, at this time, static, or very close to it, so that there is not a "linear

acceleration" component in the accelerometer measurements (in addition to the measurement of gravity). Therefore, an initial version of our orientation correction algorithm defined a parameter $0 \le \alpha \le 1$, that is derived from the "stillness" parameter ("confidence value") provided by the MARG module, and would apply the accelerometer-based correction only in proportion to α , This correction is achieved by changing the corrected orientation from the original \hat{q}_G orientation (if $\alpha=0$) to the orientation that would be predicted by the accelerometer readings alone (if α were 1), using Spherical Linear Quaternion Interpolation (SLERP) [11]. In general, the SLERP interpolation between 2 quaternions \hat{q}_0 and \hat{q}_1 will be controlled by the scalar interpolating parameter h:

$$[SLERP(q_0, q_1, h)] = \frac{q_0 \sin((1 - h)\Omega) + q_1 \sin(h\Omega)}{\sin(\Omega)}$$
(1)

where,
$$\Omega = \cos^{-1}(\hat{q}_0 \cdot \hat{q}_1)$$
 (2)

So, for example, accelerometer-based correction could be interpolated under the control of α from \hat{q}_G to \hat{q}_{GA} to define a partially corrected $\hat{q}_{partial}$:

$$\hat{q}_{\text{partial}} = [SLERP(\hat{q}_{G}, \hat{q}_{GA}, a)]$$
(3)

Since the MARG module also has a 3-axis magnetometer, a completely similar correction mechanism could be attempted on the basis of the current readings of the magnetometer. However, while the gravity acceleration vector can be properly approximated as constant throughout the working environment of the MARG module, the constant orientation of the magnetic vector in a given working environment cannot usually be assumed. This is because the magnetic field lines produced by the Earth's magnetic field will be bent, perhaps significantly, in some regions within the space in which the MARG sensor operates by the presence of ferromagnetic objects located nearby [12, 13]. The combined MARG orientation correction process we propose accepts the possibility of these magnetically distorted areas in the working space of the sensor. However, it will only apply magnetometer-based corrections when the "trustworthiness" of the magnetic field orientation currently acting on the MARG module is deemed high, as encoded in a parameter $0 \le \mu \le 1$, that will act in the same way α acted for the accelerometer-correction.

2 Methodology and Materials

Previously, an initial Gravity-Magnetic Vector Compensation (GMV) approach was introduced by O-larnnithipong [14]. That algorithm involves signals from both accelerometer and magnetometer, but under exclusive control of a single parameter, α , and does not attempt to detect magnetically distorted regions in the working space of the sensor. An accelerometer-based corrected orientation \hat{q}_{GA} is calculated and, similarly, a magnetometer-based corrected orientation, \hat{q}_{GM} is also defined. Then, GMV uses SLERP to define the final orientation quaternion between \hat{q}_{GA} and \hat{q}_{GM} , solely on the basis of α , bringing the final result closer to \hat{q}_{GA} for α closer to 1. This followed the logic that, if the MARG module is very close to a static condition, the accelerometer-based correction is trustworthy. However, if the sensor operates in a magnetically distorted

region, when simultaneously α is low, the previous method may still give \hat{q}_{GM} a large weight in the definition of the final corrected orientation estimate. This could lead to orientation estimate errors, in those particular circumstances. Our new proposed method prevents those performance shortcomings by assessing the magnetic trustworthiness, encoded in μ , and using this parameter for the quaternion interpolation also.

2.1 Double SLERP (GMV-D)

The proposed method refines the previous approach by calculating a magnetic trustworthiness parameter, μ , which is then used to control the strength of the contribution from the magnetometer-based correction into the final corrected estimate. This μ parameter has to be different for different locations around the working space of the MARG module, and it is not known for any location at the beginning of the operation of the MARG module. To keep track of the μ values at different locations, the working space is considered divided into small (e.g., 2 cm per side) cubic regions, or "voxels". Initially, all voxels are assigned a μ value of 0, since it is not known that they are magnetically trustworthy.

As the computer user proceeds to operate the system, the processing of the data from the MARG module will approximately fall into one of 4 cases at every sampling time, which are summarized in Table 1. At every sampling instant, the position of the sensor will be retrieved from the OptiTrack system and, with this and the readings from the MARG module, the control parameters α and μ will be managed and used to determine the contribution of the accelerometer-based correction and the magnetometer-based correction to the final orientation estimate.

The final orientation estimate will be calculated form 2 preliminary results, \hat{q}_{SA} and \hat{q}_{SM} , which represent the partial accelerometer-based and magnetometer-based corrections to \hat{q}_{G} , via corresponding SLERP operations:

$$\hat{q}_{SA} = SLERP(\hat{q}_G, \hat{q}_{GA}, \alpha) \tag{4}$$

$$\hat{q}_{SM} = SLERP(\hat{q}_G, \hat{q}_{GM}, \mu) \tag{5}$$

It must be noticed that, if α is low, \hat{q}_{SA} will not be much different from \hat{q}_{G} . Similarly, if μ is low, \hat{q}_{SM} will not be much different from \hat{q}_{G} .

The final orientation estimate will be obtained from a second SLERP operation on both of the preliminary results, and controlled by α :

$$\hat{q}_{OUT} = SLERP(\hat{q}_{SM}, \hat{q}_{SA}, \alpha) \tag{6}$$

Case	μ close to:	α close to:	$\hat{q}_{SM} pprox$	$\hat{q}_{S\!A} pprox$	$\hat{q}_{OUT} pprox$
Case 0	0	0	\hat{q}_G	\hat{q}_G	\hat{q}_G
Case 1	0	1	\hat{q}_G	\hat{q}_{GA}	\hat{q}_{GA}
Case 2	1	0	\hat{q}_{GM}	\hat{q}_G	\hat{q}_{GM}
Case 3	1	1	\hat{q}_{GM}	\hat{q}_{GA}	\hat{q}_{GA}

Table 1. Summarizes the differential emphasis that are given to the accelerometer-based and magnetometer-based contributions to the final orientation estimate.

2.2 The Control Parameters (α and μ)

Parameter a

Prior to being used to determine the value of the control parameter α , the average of recent stillness ("confidence") values read from the MARG module are processed by a first-order Gamma filter to smoothen the signal. The Gamma filter uses a weight parameter (W), which ranges from 0 to 1, to control the filtering characteristics of the low pass filter it implements on the signal. (We selected $W_{\alpha}=0.25$.) The first-order Gamma filter has the difference equation derived in Eqs. 7 to 10.

$$H(z) = \frac{Y(z)}{X(z)} = \frac{W}{z - (1 - W)} \tag{7}$$

$$Y(z) = (W)z^{-1}X(z) + (1 - W)z^{-1}Y(z)$$
(8)

$$y[n] = (W)x[n-1] + (1-W)y[n-1]$$
(9)

$$\alpha_g = W_\alpha(Stillness(n-1)^2) + (1 - W_\alpha)\alpha_g(n-1)$$
 (10)

Then a linear equation was applied to accelerate the drop of the α parameter when the sensor begins departing from a static status. This equation is characterized by the value of its slope (m_{α}) . The final value of the control parameter for quaternion interpolation of gravity vector correction (α) is calculated from Eqs. 11 and 12.

$$\alpha' = m_{\alpha}\alpha_g + (1 - m_{\alpha}) \tag{11}$$

$$\alpha = \alpha' + \frac{|\alpha'|}{2} \tag{12}$$

Magnetic Correction Trustworthiness (μ)

To define this Magnetic Correction Trustworthiness parameter (μ) the current position data from the OptiTrack system is used to identify in which voxel the MARG module is presently located, applying Eq. 13 for all three axes

Location of MARG module (index of voxel) =
$$floor(\frac{current\ Coordinate}{Voxel\ Size}) + 1$$
 (13)

The μ parameter will be used for the definition of the final orientation estimate, as indicated in Eqs. 4, 5, and 6. However, before every iteration (sampling instant) is ended, the current value of α is compared against a threshold, α_{TH} . If $\alpha > \alpha_{TH}$, we can expect that the correction suggested by the accelerometer, here identified as $\hat{q}_G = \hat{q}_{Gpost}$, is correct. This will provide an opportunity to update the value of μ for the current voxel.

It is possible that the μ value retrieved from memory may simply be the zero-value assigned during initialization. To update this value, we will assess the difference between the orientation estimate that would be suggested from the current magnetometer readings, m_0 and the one calculated by rotating the initial magnetic field vector, M_{int} , with the recently computed \hat{q}_{Gpost} , which we trust to be correct. To do this we compute the angle γ , whose cosine ranges from -1 to 1.

The parameter μ is computed from cosine of γ by rescaling and application of a linear equation to severely penalize departures from perfect agreement (which would yield $\mu=1$):

$$\vec{\mu}(q_{Gpost}) = q_{Gpost}^* \otimes M_{int} \otimes q_{Gpost}$$
 (14)

$$cos(\gamma) = \frac{\vec{m}_0 \vec{\mu}(q_{Gpost})}{|\vec{m}_0||\vec{\mu}(q_{Gpost})|}$$
(15)

$$\mu' = m_m(acos(cos(\gamma))) + 1 \tag{16}$$

$$\mu = \frac{(1+\mu')}{2} \tag{17}$$

It is expected that, as the user moves his/her hand through the working space of the system the initial $\mu=0$ values assigned at initialization will be updated by μ values that really reflect the magnetic trustworthiness of the regions visited by the module.

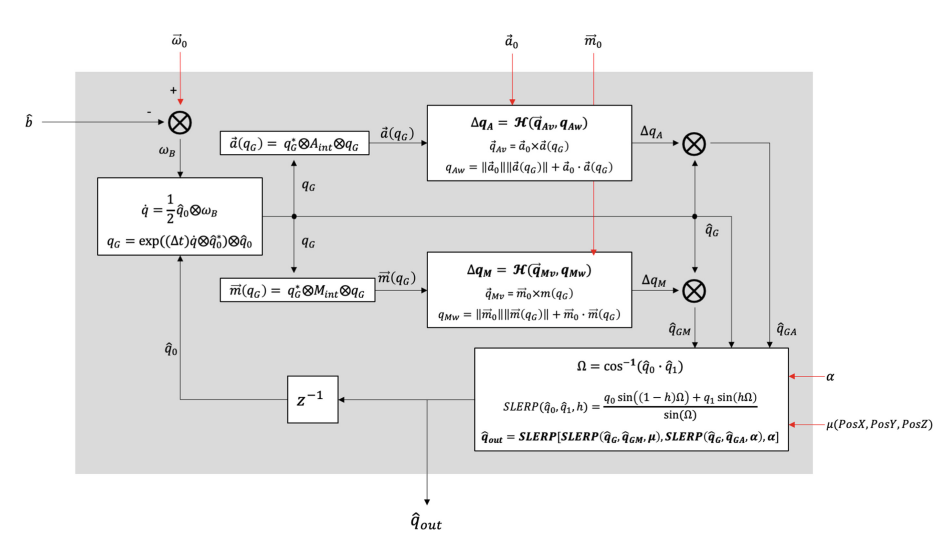


Fig. 1. Block diagram of the orientation correction algorithm using the gravity vector and magnetic North vector with Double SLERP (GMV-D).

This will enable the effective consideration of magnetometer-based correction in more instances but will prevent allowing magnetometer readings to introduce large errors where the magnetic field is distorted. The overall proposed algorithm is outlined in the block diagram shown in Fig. 1.

3 Implementation

To quantify the performance of the proposed algorithm, thirty human subjects (22 males and 8 females, all right-handed) participated in an experiment. Their ages ranged from 18 to 60 years old. None of the subjects reported any motion impediments which could affect the performance of the evaluation task. The MARG module was attached to a wooden holding box (prism) for ease of manipulation. During the performance, the locations of the holding box were recorded using the marker coordinates from the OptiTrack V120: Trio system, and the data from a Magnetic, Angular-rate, Gravity (MARG) module attached to the holding box was recorded. The orientations estimated by the methods implemented while the subjects were sustaining specific instructed poses were analyzed statistically. In the area without magnetic distortion, each subject held 9 poses (First, pose 1, then poses 2, 3, 4 and 5, with a return to Pose 1 after each). Similarly, each subject held 9 poses in the magnetically distorted area (Pose 6 and then 7, 8, 9 and 10 with returns to 6).

The proposed algorithm was implemented to calculate the estimated orientation. The calculated results obtained from the Gravity Vector and Magnetometer with Double SLERP (GMV-D) were compared with the orientation estimates obtained from the Gravity Vector and Magnetometer with Single SLERP (GMV-S), and the Kalman-based filter quaternion output that was provided directly from the Yost Labs 3-Space MARG sensor module.

3.1 Hardware and Environment Setup

The experimental space was set up, as shown in Fig. 2, with a wooden frame to prevent the presence of uncontrolled magnetic distortion in the area. An iron bar (0.5 cm \times 3.8 cm \times 37.5 cm) was placed on a wooden stool at the same height as the non-magnetic distortion area to create a magnetically distorted area. There was a docking position ("home position") where the holding box would rest before and after each trial. The initial data used in the algorithm was collected at the beginning of the experimental run, when the MARG was at the home position. The OptiTrack V120: Trio camera was placed in front of the experimental area with a PC monitor next to it. Participants followed animated on-screen instructions created in Unity software. In Fig. 3, a picture of the testing area is shown and compared to a 3D plot of the same spatial region indicating μ values detected in some voxels sampled, where blue indicates $\mu \geq 0.9$ and red represents $\mu < 0.9$.

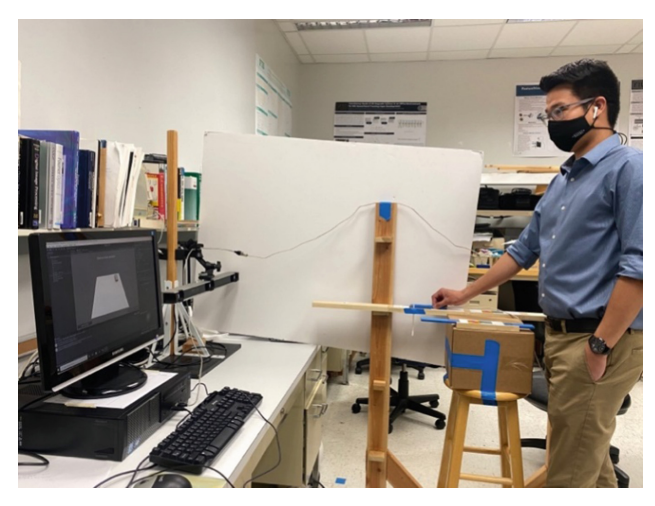


Fig. 2. The subject performs the experiment at the testing area.

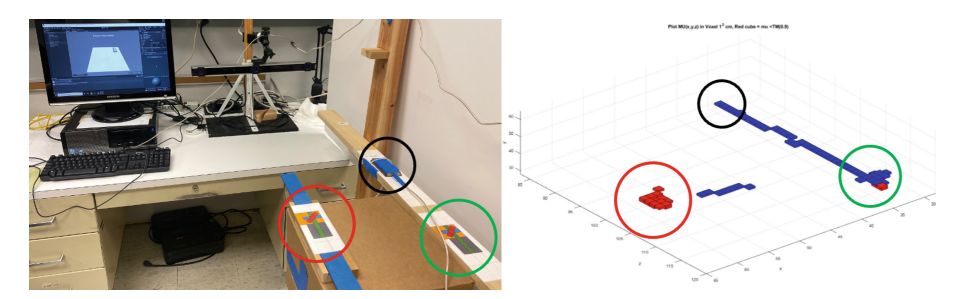


Fig. 3. The experiment station compared to a MU plot for some 3D voxels visited by the MARG. Red cubes indicate significant magnetic distortion (MU < 0.9) (Color figure online)

3.2 Software Setting

A virtual 3D environment was also created in the same project with Unity. A 3D rectangle shape was created to represent the wooden holding box. A C# script was written to predefine the movements of the sensor box that the subject had to perform. They consisted of an initial position at the dock area, nine specific orientations (or "poses") at the

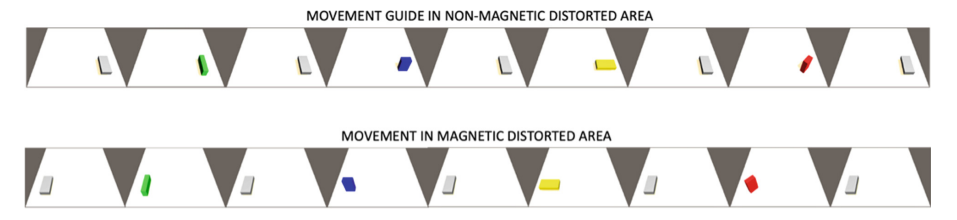


Fig. 4. The movement guide animation in non-magnetically distorted (top) and magnetically distorted (bottom) areas showing the identical rotations performed.

non-magnetic distorted area, nine poses at the magnetic distorted area, and the ending position at the dock area. The 3D box model was displayed as the movement guide for the subjects to follow and perform the experiment. The nine poses at both the non-magnetically distorted area and the magnetically distorted area are identical, as shown in Fig. 4.

3.3 Experiment Procedure

- 1. Firstly, the subject was asked to stand in the testing area, facing toward the IR camera and a desktop monitor with the holding box placed in front of him/her. Then, the experimenter started the program.
- 2. The experimenter clicked on the button "Mark this position and orientation" to record the initial position and orientation of the sensor.
- 3. The experimenter clicked on the button "Show next movement" to show the animation of the 3D box model. The 3D box model rotated and/or translated to the next state (pose) of the box movement sequence.
- 4. The subject grasped the box and moved it to match the position and orientation as shown by the movement guide on the screen.
- 5. The experimenter clicked on the button "Mark this position and orientation" to record the current position and orientation of the box.
- 6. Steps 3 to 5 were repeated until all the expected states or poses of the movement of the 3D box model had been performed by the subject.
- 7. The subject was asked to repeat the experiment two times. Then, the subject was asked to answer a simple questionnaire about age, gender, and his/her dominant hand.

4 Results and Discussion

The statistical analysis compares the performance of 3 algorithms: Kalman Filter (KF), GMV-S, and GMV-D. A total of 1620 rows of data (30 subjects x 18 orientations x 3 algorithms) were recorded and statistically analyzed using the SPSS statistical package. The recorded data represent the difference between the reference orientation (instructed to the subjects) and the output from the algorithms, measured in terms of the corresponding Euler Angles (Phi, Theta and Psi, which represent the value of the angles rotated about the x, y and z axes). If the orientation algorithm worked correctly, these differences were expected to be 'zero'. The estimated means and standard deviation of the orientation errors in all Euler Angles in both areas (with and without magnetic distortion) are shown in the Table 2. It is clear in this table that the means and standard deviation of the orientation errors for GMV-D are much less than those of the other two methods (GMV-S, KF) in every Euler Angle. Figures 5, 6 and 7 show the estimated marginal means of the orientation errors for Phi, Theta and Psi from all methods, respectively. In these figures, the integer numbers shown on the horizontal axis ("Sequence") are the numbers of the "pose" in which the subject held the MARG, at those times.

Algorithm	Dependent variable	Phi	Theta	Psi
GMV-D	Mean	1.858	8.231	3.992
	Std. deviation	2.658	10.818	8.554
GMV-S	Mean	5.053	38.318	16.104
	Std. deviation	14.769	52.557	37.527
KF	Mean	11.065	53.452	17.887
	Std. deviation	17.071	65.382	40.489
Total	Mean	5.992	33.334	12.661
	Std. deviation	13.659	52.302	32.821
	N	1800	1800	1800

Table 2. Estimated means and standard deviation of the orientation output. (in degree)

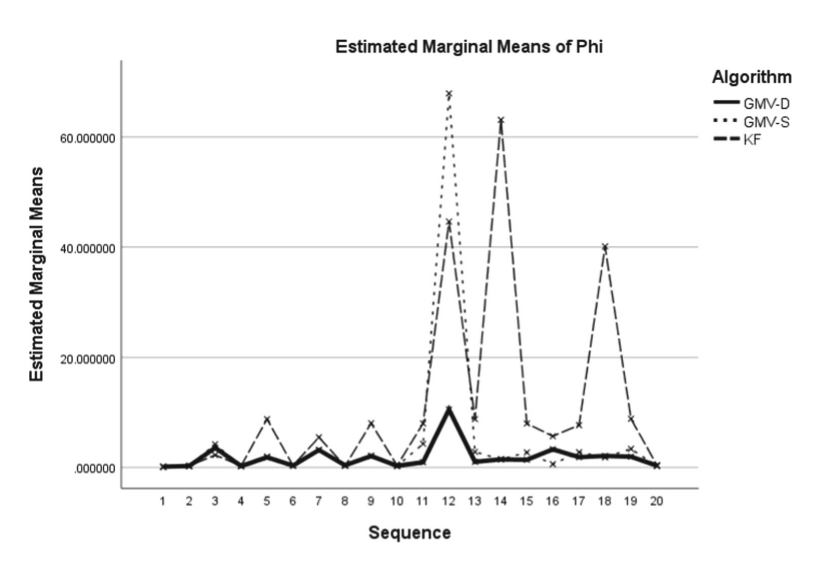


Fig. 5. Estimated marginal means of the orientation errors for Phi (in degrees)

The multivariate analysis of variance (MANOVA) was originally chosen to test for the effects of the three algorithms on the orientation output errors. However, the appropriate application of MANOVA analysis requires verification of two key assumptions in the data, which are normality of the error and equal variances across treatments. The null hypothesis for normality test is that the data are normally distributed within each treatment group. The results from the tests of normality (Kolmogorov-Smirnov and Shapiro-Wilk) are shown in Table 3 having the p-values of 0.000 for all angles and all methods. These results provided strong evidence that the orientation output errors are not normally distributed.

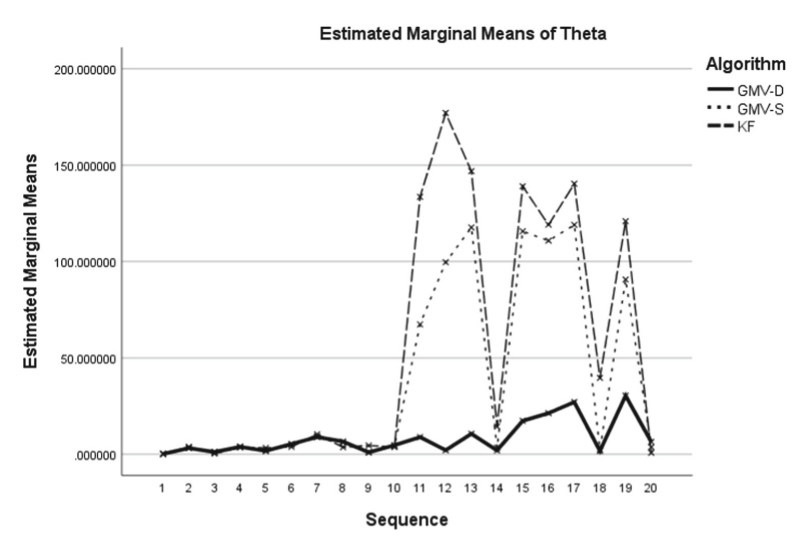


Fig. 6. Estimated marginal means of the orientation errors for Theta (in degrees)

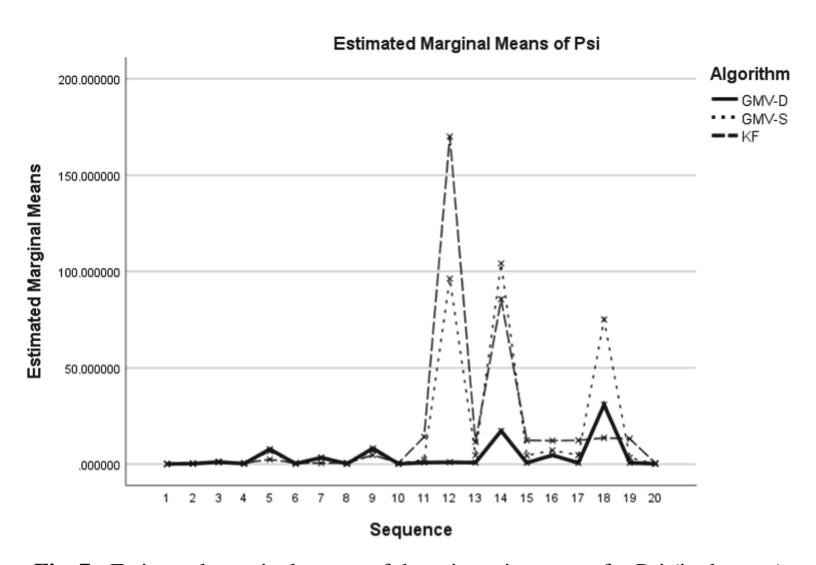


Fig. 7. Estimated marginal means of the orientation errors for Psi (in degrees)

Next, the homogeneity of variances was tested with the null hypothesis that the error variance of the dependent variable is equal across treatment groups, yielding the results shown in the Table 4. The p-values = 0.000 from all three dependent variables of the test of homogeneity of variances, provide strong evidence that the error variances are not equal among three treatment groups (GMV-D, GMV-S and KF) which, therefore, results in rejection of the null hypothesis.

		Kolmogorov-Smirnov ^a			Shapiro-Wilk			
	Algorithm	Statistic	df	Sig.	Statistic	df	Sig.	
Phi	GMV-D	.243	600	.000	.591	600	.000	
	GMV-S	.424	600	.000	.314	600	.000	
	KF	.319	600	.000	.643	600	.000	
Theta	GMV-D	.224	600	.000	.692	600	.000	
	GMV-S	.348	600	.000	.707	600	.000	
	KF	.302	600	.000	.733	600	.000	
Psi	GMV-D	.321	600	.000	.498	600	.000	
	GMV-S	.412	600	.000	.462	600	.000	
	KF	.377	600	.000	.446	600	.000	

Table 3. Tests of normality: Kolmogorov-Smirnov and Shapiro-Wilk

Table 4. Levene's test of equality of error variances.

		Lovens			
		Levene Statistic	df1	df2	Sig.
Phi	Based on Mean	24.062	59	1740	.000
	Based on Median	21.110	59	1740	.000
	Based on Median and with adjusted df	21.110	59	131.746	.000
	Based on trimmed mean	22.299	59	1740	.000
Theta	Based on Mean	61.970	59	1740	.000
	Based on Median	37.068	59	1740	.000
	Based on Median and with adjusted df	37.068	59	193.641	.000
	Based on trimmed mean	58.456	59	1740	.000
Psi	Based on Mean	105.361	59	1740	.000
	Based on Median	64.094	59	1740	.000
	Based on Median and with adjusted df	64.094	59	96.072	.000
	Based on trimmed mean	103.864	59	1740	.000

Dependent variable: Phi, Theta, Psi

Design: Intercept + Algorithm + Sequence + Algorithm * Sequence

As the MANOVA analysis was found not to be appropriate for the data, the non-parametric Kruskal-Wallis H test was chosen to perform the analysis, since it does not require the assumptions of variance homogeneity and normality of errors [15]. The Kruskal-Wallis is a rank-based nonparametric test, commonly used for determining the statistical significance of the differences of a dependent variable across two or more treatment groups [16]. Each dependent variable (Phi, Theta and Psi) was tested with the

a. Lilliefors Significance Correction

Kruskal-Wallis approach at a level of significance of 0.05 to determine if there are differences in means across the three algorithms (treatments). The analysis was performed separately for the poses held in the area that was not magnetically disturbed (Sequence number 2 to 10) and the area that was magnetically disturbed (Sequence number 11 to 19).

For the area, which was not magnetically distorted, Table 5 shows that the distributions of both Phi and Theta were not significantly different across the three algorithms, with H = 5.478, p = 0.065 and H = 2.439, p = 0.295, respectively. The null hypothesis that the distribution of orientation errors is the same across algorithms was rejected only for the Psi angle, for which H(2) = 14.586, p = 0.001, with a mean rank of 381.70 for GMV-S, 384.93 for GMV-D and 449.86 for KF. Through pairwise comparisons, as shown in Table 6, the results indicate that there are no statistically significant differences of the orientation errors in Psi between GMV-S and GMV-D (p = 1.000) while KF shows statistically significant differences of the orientation errors with GMV-S (p = 0.002) and GMV-D (p = 0.004).

Table 5.	Kruskal-Wallis	test statistics i	results for the	e orientation	errors in the	Euler angle Phi,
Theta an	d Psi across three	e different meth	hods in the no	n-magnetical	ly distorted a	area with $N = 810$

Dependent variable	Algorithm	Mean rank	Test statistic	Df	Asymp. Sig.
Phi	GMV-D	_	5.478	2	0.065
	GMV-S	_			
	KF	_			
Theta	GMV-D	_	2.439	2	0.295
	GMV-S	_			
	KF	_			
Psi	GMV-D	384.93	14.586	2	0.001
	GMV-S	381.70			
	KF	449.86			

Table 6. Pairwise comparison among three algorithms for orientation errors in the Euler angles Psi in the non-magnetically distorted area.

Algor 1–Algor 2	Test statistic	Std. error	Std. test statistic	Sig.	Adj. sig.
GMV-S-GMVD	3.230	20.137	0.160	0.873	1.000
GMV-S-KF	-68.159	20.137	-3.385	0.001	0.002
GMV-D-KF	-64.930	20.137	-3.224	0.001	0.004

¹ Each row tests the null hypothesis that the Sample 1 and Sample 2 distributions are the same. Asymptotic significance (2-sided tests) is displayed. The significance level is .05.

For the area affected by magnetic distortion, Table 7 shows the test summary, which leads to rejection of the null hypothesis that the distribution of orientation errors for all the angles (Phi, Theta and Psi) is the same across algorithms. Table 8 supplements the information by showing the statistics for pairwise comparisons among algorithms, regarding their error levels on Phi, Theta and Psi.

With respect to Phi, Table 7 shows results that lead to the rejection of the null hypothesis (that the distribution of Phi errors is the same across the algorithms). The results from the test indicate that there is a statistically significant difference between the orientation errors in Phi produced by different algorithms (H(2) = 365.929, p = 0.000), with a mean rank of 252.20 for GMV-D, 342.62 for GMV-S and 621.69 for KF. Through pairwise comparisons among the three algorithms, it was found that there are statistically significant differences of the orientation errors in Phi between GMV-D and GMV-S (p = 0.000), between GMV-D and KF (p = 0.000), and between GMV-S and KF (p = 0.000). GMV-D shows the best performance, which is 4.490 less than GMV-S and 18.349 less than KF, in standard test statistic value. With respect to Theta, Table 7 shows results that lead to the rejection of the null hypothesis (that the distribution of Theta errors is the same across the algorithms). The results from the test indicate that there is a statistically significant difference between the orientation errors in Theta produced by the different algorithms (H(2) = 377.616, p = 0.000), with a mean rank of 197.76 for GMV-D, 432.47 for GMV-S and 586.27 for KF. Through pairwise comparisons among the three algorithms, it was found that there are statistically significant differences of the orientation errors in Theta between GMV-D and GMV-S (p = 0.000), between GMV-D and KF (p = 0.000), and between GMV-S and KF (p = 0.000). GMV-D shows the best performance, which is 11.656 less than GMV-S and 19.293 less than KF in standard test statistic value. Lastly, with respect to Psi, Table 7 shows results that lead to the rejection of the null hypothesis (that the distribution of Psi errors is the same across the algorithms). The results from the test indicate that there is a statistically significant difference between the orientation errors in Psi for different algorithms (H(2) = 278.583, p = 0.000), with a mean rank of 229.84 for GMV-D, 421.93 for GMV-S and 564.73 for KF. Through pairwise comparisons among the three algorithms, it was found that there are statistically significant differences of the orientation errors in Psi between GMV-D and GMV-S (p = 0.000), between GMV-D and KF (p = 0.000), and between GMV-S and KF (p = 0.000). GMV-D shows the best performance, which is 9.539 less than GMV-S and 16.631 less than KF in standard test statistic value.

The preceding sections, overall, have shown results that match the key intent of the development of the newly proposed algorithm, GMV-D, which was to make the orientation estimation derived from signals of the MARG module more robust in circumstances where distortion of the geomagnetic field exist. The evaluation procedure was defined in such a way that its first half would take place within a region of space where the geomagnetic field was not distorted (non-magnetically distorted area), whereas the second half took place in the immediate neighborhood of the iron bar, which was known to introduce significant distortion of the magnetic field (magnetically distorted area).

Table 7. Kruskal-Wallis test statistics results for the orientation errors in the Euler angle Phi,
Theta and Psi across three different methods in the magnetically distorted area with $N=810$.

Dependent variable	Algorithm	Mean rank	Test statistic	Df	Asymp. Sig.
Phi	GMV-D	252.20	365.929	2	0.000
	GMV-S	342.62			
	KF	621.69			
Theta	GMV-D	197.76	377.616	2	0.000
	GMV-S	432.47			
	KF	586.27			
Psi	GMV-D	229.84	278.583	2	0. 000
	GMV-S	421.93			
	KF	564.73			

Table 8. Pairwise comparison among three algorithms for orientation errors in the Euler angles in the magnetically distorted area.

Dependent variable	Algor 1–Algor 2	Test statistic	Std. error	Std. test statistic	Sig.	Adj. sig.
Phi	GMV-D-GMV-S	-90.422	20.137	-4.490	.000	.000
	GMV-D-KF	-369.489	20.137	-18.349	.000	.000
	GMV-S-KF	-279.067	20.137	-13.858	.000	.000
Theta	GMV-D-GMV-S	-234.711	20.137	-11.656	.000	.000
	GMV-D-KF	-388.511	20.137	-19.293	.000	.000
	GMV-S-KF	-153.800	20.137	-7.638	.000	.000
Psi	GMV-D-GMV-S	-192.093	20.137	-9.539	.000	.000
	GMV-D-KF	-334.896	20.137	-16.631	.000	.000
	GMV-S-KF	-142.804	20.137	-7.092	.000	.000

For a human-computer interface purpose, it was necessary to evaluate the results accounting for the diversity of trajectories, movement speed, etc. that various human subjects would use in completing the experimental task. To investigate the deviations of those recorded orientations from the "instructed orientations" ("ground truth") and in order to report the results in a more intuitive way, the orientation errors were expressed as Euler Angles, which are the errors around the 3 orthogonal axes of the "body frame" of the MARG module. These angles (Phi, Theta and Psi) are the angles rotated about the x, y, and z axes, and can, therefore, be more readily interpreted than the 4 numerical components of a quaternion [17]. Since the analysis was performed on angular errors,

a lower mean value found for a given method than for another implies that the former performed better that the latter.

5 Conclusion

The statistical analyses show that the new algorithm (GMV-D) performance was similar to the performance of the previous algorithm (GMV-S) and both were slightly better than the on-board Kalman Filtering in the non-magnetically distorted area. However, the GMV-D algorithm can significantly reduce the errors in orientation tracking when compared to the GMV-S correction and Kalman filtering correction in the magnetically distorted area.

The advancement of hand motion tracking systems using MARG modules and infrared cameras can be a valuable contribution to the improvement in the realism of natural human-computer interactions within a 3D virtual environment.

Acknowledgments. This research was supported by National Sciences Foundation grants CNS-1532061 and CNS-1920182, and the FIU University Graduate School Dissertation Year Fellowship awarded to Dr. Neeranut Ratchatanantakit.

References

- 1. Kim, S.J.J.: A user study trends in augmented reality and virtual reality research: a qualitative study with the past three years of the ISMAR and IEEE VR conference papers. In: 2012 International Symposium on Ubiquitous Virtual Reality, pp. 1–5. IEEE, August 2012
- Heeter, C.: Being there: the subjective experience of presence. Teleoper. Virtual Environ. 1(2), 262–271 (1992). https://doi.org/10.1162/pres.1992.1.2.262
- 3. Mccall, R., O'Neil, S., Carroll, F.: Measuring presence in virtual environments. ACM (2004). ID: acm985934; ACM Digital Library; ACM Digital Library (Association for Computing Machinery); KESLI (ACM Digital Library)
- Slater, M., Usoh, M., Steed, A.: Depth of presence in virtual environments. Teleoper. Virtual Environ. 3(2), 130–144 (1994)
- 5. Slater, M., Wilbur, S.: A framework for immersive virtual environments (five). Teleoper. Virtual Environ. **6**(6), 603 (1997)
- Pavlovic, V.I., Sharma, R., Huang, T.S.: Visual interpretation of hand gestures for humancomputer interaction: a review. IEEE Trans. Pattern Anal. Mach. Intell. 19(7), 677–695 (1997)
- 7. Roh, M.-C., Kang, D., Huh, S., Lee, S.-W.: A virtual mouse interface with a two-layered Bayesian network. Multimedia Tools Appl. **76**(2), 1615–1638 (2017). ID: Roh 2017
- 8. Zhang, X., Liu, X., Yuan, S.-M., Lin, S.-F.: Eye tracking based control system for natural human-computer interaction. Comput. Intell. Neurosci. (2017)
- Ratchatanantakit, N., O-larnnithipong, N., Sonchan, P., Adjouadi, M., Barreto, A.: Live demonstration: double SLERP gravity-magnetic vector (GMV-D) orientation correction in a MARG sensor. In: 2021 IEEE Sensors, p. 1. IEEE (2021)
- Foxlin, E.: Motion tracking requirements and technologies (Chapter 8). In: Stanney, K. (ed.)
 Handbook of Virtual Environments: Design, Implementation, and Applications, pp. 163–201.
 Lawrence Erlbaum Associates, New York (2002)
- 11. Shoemake, K.: Animating rotation with quaternion curves. In: Proceedings of the 12th Annual Conference on Computer Graphics and Interactive Techniques, pp. 245–254, July 1985

- 12. Bachmann, E.R., Yun, X., Peterson, C.W.: An investigation of the effects of magnetic variations on inertial/magnetic orientation sensors. In: IEEE International Conference on Robotics and Automation, Proceedings. ICRA 2004, vol. 2, pp. 1115–1122. IEEE, April 2004
- 13. Ratchatanantakit, N., O-larnnithipong, N., Barreto, A., Tangnimitchok, S.: Consistency study of 3D magnetic vectors in an office environment for IMU-based hand tracking input development. In: Kurosu, M. (ed.) HCII 2019. Lecture Notes in Computer Science, vol. 11567, pp. 377–387. Springer, Cham (2019). https://doi.org/10.1007/978-3-030-22643-5_29
- O-larnnithipong, N., Barreto, A., Tangnimitchok, S., Ratchatanantakit, N.: Orientation correction for a 3D hand motion tracking interface using inertial measurement units. In: Kurosu, M. (ed.) HCI 2018. Lecture Notes in Computer Science, vol. 10903, pp. 321–333. Springer, Cham (2018). https://doi.org/10.1007/978-3-319-91250-9 25
- 15. Montgomery, D.C.: Design and Analysis of Experiments. Wiley, New York (2017)
- 16. Field, A.: Discovering Statistics Using SPSS. Sage Publications, Upper Saddle River (2009)
- 17. Kuipers, J.B.: Quaternions and Rotation Sequences: A Primer with Applications to Orbits, Aerospace, and Virtual Reality. Princeton University Press, Princeton (1999)